*Int. J. Multiphase Flow* Vol. 4, pp. 279–302

0301-9322/78/0601-0279/$02.00/0

# MODES OF BUBBLE GROWTH IN THE SLOW-FORMATION REGIME OF NUCLEATE POOL BOILING

A. K. CHESTERS
Laboratory for Aero- and Hydrodynamics, Delft University of Technology, The Netherlands

(*Received* 10 *April* 1977)

**Abstract**—The shape and size of a bubble formed slowly on a sharp- or round-edged orifice are derived with the help of a new analytical solution for the bubble profile. Two modes of formation are distinguished, depending on the natural contact angle, $\varphi_0$: bubble confined to the orifice ($\varphi_0$ small); bubble spreading beyond the orifice ($\varphi_0$ large : Fritz mode). The limits of the slow-formation regime in nucleate pool boiling are estimated, involving an assessment of the influences of liquid inertia, viscosity and surface-tension gradients.

"Slow" formation is predicted for large cavities or high pressures and this is borne out by data for water. The Fritz mode of growth, however, is seen to be suppressed.

## 1. INTRODUCTION

This size and shape of vapour bubbles formed on a horizontal heated surface in nucleate pool boiling are affected by so many factors that a general description would be very complex and is certainly not available at the present time. These factors include gravity, surface tension, contact angle, geometry of the heated surface, thermal properties, inertia and viscosity of both phases and gradients of temperature and so of physical properties. Under certain conditions however the influences associated with the *rate* of growth may be expected to become minor and the size and shape at detachment should then be governed by the first four "static" factors.

The character and limits of this "slow-formation" regime are examined below and the results compared with experiment. The case of slow, isothermal growth on a sharp-edged orifice is considered first, since this case is now fairly thoroughly understood. It is seen that there are two possible modes of growth: mode A, in which the bubble boundary is the cavity edge, and mode B, in which the bubble spreads beyond the cavity. Which mode occurs depends on the magnitude of the contact angle. Bubble volume formulae are obtained for both modes, that for mode B providing an analytical justification of the well-known Fritz formula. The case of a round-edged orifice is also analyzed, after which the limits of the slow-formation regime are examined.

Comparison with pool boiling results for water largely corroborates the expectations but yields the unexpected result that mode B growth, on which so many heat-transfer correlations are based, does not occur in the cases examined, despite authors' contentions to the contrary. This is attributed to the slowness with which a contact angle attains its equilibrium value.

## 2. SIZE AND SHAPE OF BUBBLES FORMED SLOWLY ON A ROUND, SHARP-EDGED, HORIZONTAL ORIFICE UNDER ISOTHERMAL CONDITIONS

### *Bubble shape*

Provided flow into or out of the bubble is sufficiently slow, the associated pressure variations and viscous stresses are negligible and the pressure variation in the two fluids is simply that required to balance gravitational forces:

$$p_G = \rho_G g Y + \text{const.}, \qquad [1]$$

$$p_L = \rho_L g Y + \text{const.} \qquad [2]$$

where $p$, $g$ and $Y$ denote respectively pressure, acceleration due to gravity and distance

measured vertically downwards from the bubble apex (figure 1, which also defines $X$), and the suffixes $G$ and $L$ refer to gas and liquid. The interface condition is

$$p_G - p_L = \sigma\left(\frac{1}{R_a} + \frac{1}{R_b}\right) \qquad [3]$$

where viscous stresses have again been neglected and $\sigma$ denotes the (constant) surface tension, $R_a$ is the radius of curvature of the interface in the plane of the $Y$ axis and $R_b$ that in the perpendicular plane containing the normal.

Elimination of $p_G$ and $p_L$ from [1] to [2], together with the requirement that $R_a = R_b = R$ (the radius of curvature of the bubble apex) at $Y = 0$, yields

$$\sigma\left(\frac{1}{R_a} + \frac{1}{R_b}\right) = \frac{2\sigma}{R} - \rho g Y \qquad [4]$$

where

$$\rho = \rho_L - \rho_G. \qquad [5]$$

Substitution of the appropriate expressions for $R_a$ and $R_b$ yields the following ordinary differential equation for the bubble profile:

$$\frac{\dfrac{d^2Y}{dX^2}}{\left[1+\left(\dfrac{dY}{dX}\right)^2\right]^{3/2}} + \frac{\dfrac{1}{X}\dfrac{dY}{dX}}{\left[1+\left(\dfrac{dY}{dX}\right)^2\right]^{1/2}} = \frac{2}{R} - \frac{\rho g Y}{\sigma} \qquad [6]$$

or, in terms of the dimensionless coordinates $x(= X/R)$ and $y(= Y/R)$,

$$\frac{\dfrac{d^2y}{dx^2}}{\left[1+\left(\dfrac{dy}{dx}\right)^2\right]^{3/2}} + \frac{\dfrac{1}{x}\left(\dfrac{dy}{dx}\right)}{\left[1+\left(\dfrac{dy}{dx}\right)^2\right]^{1/2}} = 2 - \beta y \qquad [7]$$

where

$$\beta = \rho g R^2/\sigma. \qquad [8]$$

The dimensionless parameter $\beta$ thus evidently determines the shape of the profile while $R$ determines the scale.

The only exact analytical solution of [7] is for $\beta = 0$ (corresponding to zero gravity) when, as expected, the profile is a circle. Numerical solutions exist for various $\beta$ values (Hartland & Hartley 1976) and an analytical solution which is a good approximation if

$$\beta \leq 0.1 \qquad [9]$$

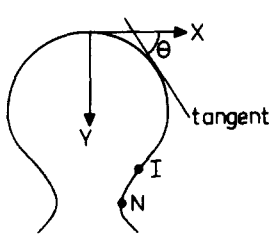


Figure 1. Choice of coordinate system.

has recently been obtained by the author (Chesters 1977). Since [9] is satisfied in many boiling situations† this approximate analytical solution is assumed to apply in what follows unless otherwise stated.

The type of profile obtained is illustrated in figure 2 for the case $\beta = 0.0955$. The points represent the numerical solution of Hartland & Hartley (1976). The profile is seen to resemble a circle closely up to the underside where it deflects away from the $Y$ axis to form a neck. In the neck region ($x \lesssim \sqrt{\beta}$) the variation of $\theta$ ($= \tan^{-1}(dY/dX) = \tan^{-1}(dy/dx)$: figure 1 with $x$ is given to the first order in $\beta$ by

$$\sin\theta = x + 2\beta/3x, \qquad [10]$$

from which follows

$$x_I = \sqrt{(2\beta/3)}, \qquad [11]$$

$$\sin\theta_I = 2\sqrt{(2\beta/3)} \quad \text{(radians)}. \qquad [12]$$

and

$$x_N = 2\beta/3 \qquad [13]$$

where $I$ and $N$ are respectively the inflexion point (where $d\theta/dx = 0$) and the neck point (where $\theta = 90°$): figure 1. The volume, $V$, of the bubble above any horizontal plane cutting the profile in the neck region is

$$V = \frac{4}{3}\pi R^3(1+\beta) \qquad [14]$$

to the first order in $\beta$.

*Boundary conditions*

The equilibrium of the contact line between a gas, a liquid and a solid plane (figure 3a) requires equilibration of the three interfacial tensions which are associated with the corresponding interfacial free energies (Davies & Rideal 1963):

$$\sigma' + \cos\varphi_0 = \sigma''.$$

Since the three $\sigma$ are fixed for given media, so is $\varphi_0$, the natural contact angle.

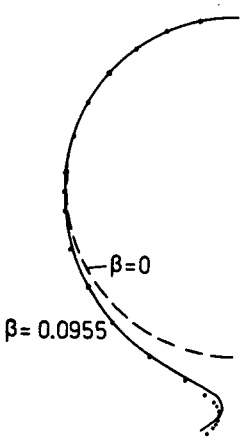


Figure 2.

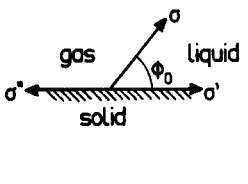


Figure 3a.

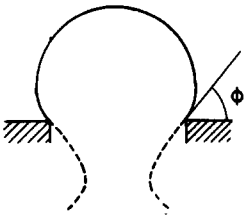


Figure 3b.

Figure 2. Analytical (—Chesters 1977) and numerical (Hartland & Hartley 1976) solutions for the bubble profile.

Figure 3. Contact angle at a solid plane, (a) with and (b) without a sharp edge.

†For water at 100°C, for example, [9] requires that $2R \lesssim 1.6$ mm.

The exception to this statement is when the solid terminates in a sharp edge (figure 3b) when any value of the contact angle $\varphi$ greater than $\varphi_0$ is found to be stable. As noted elsewhere (Chesters 1977) the explanation is probably that the actual contact line stabilizes itself a microscopic distance $\delta$ (of the order of the range of the intermolecular attraction forces) away from the edge, so that $\sigma''$ depends on $\delta$. The smaller $\delta$, the smaller $\sigma''$ and the larger $\varphi$. $\varphi = \varphi_0$, however, corresponds to $\delta = \infty$ and values of $\varphi$ less than $\varphi_0$ cannot be maintained but result in macroscopic motion of the contact line away from the edge until $\varphi$ becomes equal to $\varphi_0$.

The two related modes of growth are illustrated in figures 4a and 4b. If, during the growth process, $\varphi$ falls to $\varphi_0$, spreading occurs (mode B).

*Bubble size at detachment: mode A*

When growth occurs according to mode A (figure 4a), the scale of the profile (i.e. the value of $R$) reaches a maximum when the plane of attachment reaches the point $N$. Displacement of the plane of attachment beyond $N$ diminishes the volume enclosed by the profile above $N$. Unless this diminution is compensated by a greater increase in the volume enclosed below $N$ (the shaded zone in figure 4a), the maximum volume has been reached and the bubble detaches†. For small values of $\beta$ this situation occurs when the plane of attachment is just beyond, but very close to, the point $N$ (Chesters 1977). The maximum volume is thus given by [14], while [13] yields

$$x_N = \frac{r}{R} = \frac{2\beta}{3} \qquad [15]$$

where $r$ is the radius of the orifice. Equation [15] can be written

$$R^3 = 3r\sigma/2\rho g. \qquad [16]$$

Substituting [16] in [14] the maximum volume of the bubble is seen to be given to the first approximation by

$$V_{\max} = \frac{2\pi r\sigma}{\rho g} \qquad [17]$$

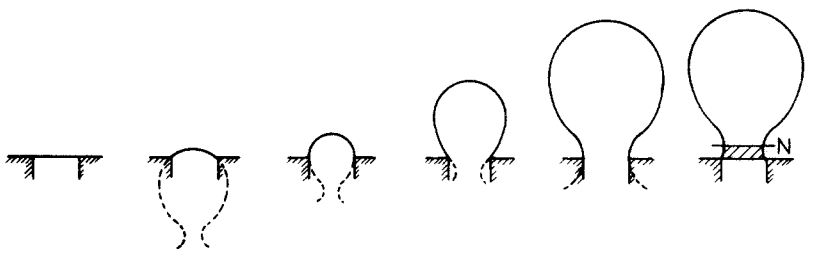


Figure 4a. Mode A bubble growth.

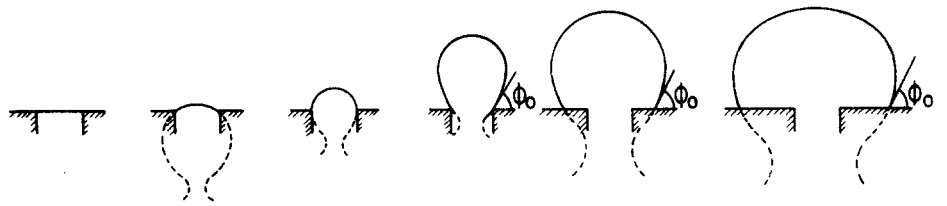


Figure 4b. Mode B bubble growth.

†On orifices of radius greater than $3.219(\sigma/\rho g)^{1/2}$ detachment occurs at an earlier stage of growth due to an instability of the profile to small perturbations: Pitts (1976), Michael & Williams (1976). However, since this critical orifice radius is of the order of 1 cm, this mechanism is not relevant to the present considerations.

or

$$\frac{V_{max}}{a^3} = 2\pi \frac{r}{a} \qquad [18]$$

where $a$ is the capillary length

$$a = \sqrt{(\sigma/\rho g)} = R/\sqrt{\beta}. \qquad [19]$$

A more accurate expression for $V_{max}$ can be obtained from a force balance since $\varphi = 90°$ very nearly at detachment (Chesters 1977), but for the present purposes [17] suffices.

The volume of the bubble which detaches is slightly less than $V_{max}$ since a volume, $V_{res}$, of the order of $r^3$ remains attached to the orifice: Vacek & Nekovar (1973). However, since from [15] $r/R = 0(\beta)$ and from [14] $V_{max} = 0(R^3)$,

$$V_{res}/V_{max} = 0(\beta^3) \qquad [20]$$

and the required correction is negligible for small bubbles.

*Bubble size at detachment: mode B*

Before determining $V_{max}$ for mode B growth (figure 4b), it is of interest to see what is the minimum value of $\varphi$ reached during mode A growth. Assuming $\varphi_{min}$ to be reached when the plane of attachment is in the neck region, [10] is applicable:

$$\sin\theta = \sin(\pi - \varphi) = \sin\varphi = \frac{X}{R} + \frac{2\beta R}{3X}. \qquad [21]$$

Since $X = r$ = constant, $\varphi_{min}$ occurs when

$$d(\sin\varphi) = 0 = \left(\frac{-r}{R^2} + \frac{2\beta}{r}\right) dR,$$

making use of [8], i.e.

$$r/R = x = \sqrt{(2\beta)} = \sqrt{3}\, x_I. \qquad [22]$$

This is indeed the neck region ($x \lesssim \sqrt{\beta}$) and substitution of [22] in [21] yields

$$\sin\varphi_{min} = \frac{4}{3}\sqrt{(2\beta)} = \frac{4}{3}\sqrt{2}\frac{R}{a}, \qquad [23]$$

making use of [19]. Since further, from [19] and [22],

$$R^2 = ra/\sqrt{2}, \qquad [24]$$

[23] may be re-written

$$\sin\varphi_{min} = \frac{4}{3} \times 2^{1/4}\sqrt{\frac{r}{a}} \qquad [25]$$

For water–water vapour at 100°C and $r = 10\,\mu$, for example, [25] gives $\varphi_{min} = 5{\cdot}44'$ (the corresponding value of $\beta$ is found from [23] to be 0.003, thus amply satisfying[9]. If $\varphi_0$ is greater

than this angle therefore the bubble boundary will move outside the orifice during growth. However, as will be seen, it may contract into the orifice again before $V_{max}$ is reached.

Assuming growth to proceed according to mode B until $V_{max}$ is reached and assuming this situation to occur when the plane of attachment is in the neck region, [14] yields

$$dV = 0 = \frac{4}{3}\pi[3R^2(1+\beta) + R^3\,d\beta] = \frac{4}{3}\pi R^2(3+5\beta)\,dR \qquad [26]$$

since, from [8],

$$d\beta/\beta = 2dR/R. \qquad [27]$$

Equation [26] indicates that at the maximum volume,

$$dR = 0 \qquad [28]$$

and differentiation of [21] making use of [28] and the fact that $\varphi = \varphi_0 = \text{constant}$ yields

$$0 = \left(\frac{1}{R} - \frac{2\beta R}{3X^2}\right) dX,$$

$$\text{i.e.} \quad x = \sqrt{(2\beta/3)} = x_I. \qquad [29]$$

This confirms the assumption that the plane of attachment lies in the neck region, this plane in fact being located at the inflexion point $I$ (figure 1). Substitution of [29] in [21] yields

$$\sin\varphi_0 = 2\sqrt{(2\beta/3)}. \qquad [30]$$

Hence $\varphi_0$ is small and, to the first order in $\beta$, [30] becomes

$$\varphi_0 = 2\sqrt{\left(\frac{2\beta}{3}\right)} = 2\sqrt{\left(\frac{2}{3}\right)}\frac{R}{a} \quad \text{radians} \qquad [31]$$

or

$$\frac{2R}{a} = \frac{\pi}{180}\sqrt{\left(\frac{3}{2}\right)}\varphi_0 = 0.0214\,\varphi_0 \qquad [32]$$

if $\varphi_0$ is in degrees. This result was first obtained by Fritz (1935), who found 0.0208 as constant, based on the numerical results of Bashforth & Adams (1883).

The corresponding bubble volume is obtained by substituting [32] in [14]:

$$\frac{V_{max}^{1/3}}{a} = 0.0172\,\varphi_0 \quad (\varphi_0 \text{ in degrees}) \qquad [33]$$

to the first approximation. Again, the volume left attached to the orifice may in general be expected to be negligible so that [33] is also an expression for the volume of the departing bubble.

The final contact radius, $r_B$, is found from [29], [30] and [19]:

$$\frac{r_B}{a} = \sqrt{\left(\frac{3}{32}\right)}\sin^2\varphi_0, \qquad [34]$$

$r_B$ is somewhat less than the critical orifice radius at which expansion outside the orifice first

begins to take place (given by [25] with $\varphi_{min} = \varphi_0$). This is because $r_B$ is not, in fact, the greatest radius reached by the bubble during mode B growth. The greatest radius, $r_{max}$, is readily seen (by differentiating [21] and putting $dX = 0$) to be given by [22], leading to an expression like [25]:

$$\frac{r_{max}}{a} = \frac{9}{16\sqrt{2}} \sin^2 \varphi_o. \qquad [35]$$

The last stage of mode B growth thus involves the shrinkage of the contact radius from $r_{max}$ to $r_B$ while $V$ (and hence $R$) continues to increase. The criterion for mode B growth to proceed to detachment so that [33] applies is thus:

$$r < r_B,$$

i.e.

$$\frac{r}{a} < \sqrt{\left(\frac{3}{32}\right)} \sin^2 \varphi_0, \qquad [36]$$

from [34]. For the previous example of water–water vapour at 100°C and $r = 10\ \mu$, [36] leads to $\varphi_0 > \sim 7°$.

Expression [33] for the final bubble volume in mode B growth is of course only reliable up to $\beta \sim 0.1$, that is, from [30], up to $\varphi_0 \sim 30°$.

## 3. THE INFLUENCE OF ROUNDING OF THE ORIFICE EDGE

The situation considered is depicted in figure 5. At all stages of growth the bubble surface joins the orifice surface at the natural contact angle $\varphi_0$ so that

$$\varphi = \varphi_0 + \alpha, \qquad [37]$$

where $\alpha$ is the inclination of the orifice surface to the horizontal in the plane of attachment. Again assuming this plane to lie in the neck region of the profile at detachment, the volume enclosed by the profile above this plane is given by [14]. The variable volume in the orifice beneath the plane of attachment may be neglected since, like the volume left behind at detachment, it is of the order of (orifice radius)$^3$. The condition that the volume be a maximum is thus once more [28], and differentiation of [21] making use of this condition yields

$$\cos \varphi \, d\varphi = \left(\frac{1}{R} - \frac{2\beta R}{3X^2}\right) dX. \qquad [38]$$

Since

$$\frac{dX}{d\varphi} = \frac{dX}{d\alpha} = -r_c \cos \alpha, \qquad [39]$$

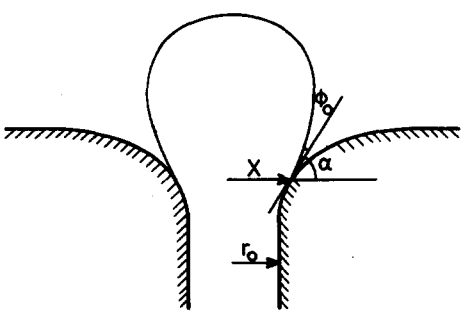


Figure 5. Bubble growth on a round-edged orifice.

where $r_c$ is the radius of curvature of the orifice surface in the plane of attachment, [38] can be written

$$\frac{X}{r_c \cos\alpha} = \frac{1}{\cos\varphi}\left(\frac{2\beta}{3x} - x\right). \qquad [40]$$

The L.H.S. of [40] is a function of the geometry of the orifice. For an orifice of the type depicted in figure 5, $r_c \to \infty$ as $\alpha \to 0°$ or 90°, while for $\alpha = 45°$, $r_c \sim X$. These general characteristics are obtained if the following relation holds:

$$\frac{r_c}{X} = \frac{1}{k \cos\alpha \sin\alpha}, \qquad [41]$$

where $k$ is a constant of the order of unity. Making use of [39], [41] in fact integrates to

$$X = r_0[\tan(\alpha/2)]^{-1/k}, \qquad [42]$$

where $r_0$ is the radius of the cylindrical region of the orifice where $\alpha = 90°$. Substitution of [41] in [40], making use of [21] yields

$$k \sin\alpha \cos\varphi = (2\beta/3x) - x = \sin\varphi - 2x. \qquad [43]$$

Squaring [43], a quadratic equation for $\sin\varphi$ is obtained, leading to

$$\sin\varphi = \frac{2x \pm \sqrt{(4x^2 + (k^2\sin^2\alpha - 4x^2)(1 + k^2\sin^2\alpha))}}{1 + k^2\sin^2\alpha}. \qquad [44]$$

Provided

$$k \sin\alpha \gg 2x \quad \text{(i.e. } k\sin\alpha \geq 1), \qquad [45]$$

equation [44] simplifies to

$$\sin\varphi = \frac{k\sin\alpha}{\sqrt{(1 + k^2\sin^2\alpha)}} \qquad [46]$$

If however

$$k \sin\alpha \ll 2x, \qquad [47]$$

[43] simplifies to

$$\sin\varphi = 2x. \qquad [48]$$

The questions to be answered are: (1) Does the bubble still spread beyond the orifice (mode B growth) if $\varphi_0$ is large enough to satisfy [36], the relevant value of $r$ now being a radius at which $\alpha \simeq 0$ (i.e. $\alpha \ll \varphi_0$)? (2) Does a bubble grow larger in the well-wetted case ($\varphi_0 = 0$, say) than it would on a sharp-edged orifice of radius $r_0$?

Beginning with the first question, when $\alpha \simeq 0$ [47] is satisfied and hence [48] applies. How small $\alpha$ has to be is seen by re-substituting [48] in [47]:

$$k\sin\alpha \ll \sin\varphi, \qquad k\alpha \ll (\varphi_0 + \alpha), \qquad (k-1)\alpha \ll \varphi_0, \qquad \text{i.e.} \quad \alpha \ll \varphi_0 \qquad [49]$$

if $k-1=0(1)$. Substitution of [48] in [21] yields

$$x=\sqrt{(2\beta/3)}=x_I \qquad [50]$$

([11]). This is indeed the solution for mode B growth ([29]) and leads to the same requirement, namely [36].

Turning to question 2, if $\varphi_0=0$ then $\varphi=\alpha$ and [46] simplifies to

$$\sin^2\varphi=(k^2-1)/k^2. \qquad [51]$$

Equation [51] indicates that if $k=\infty$, corresponding to a sharp edge, $\varphi=90°$ and from [21] $x=2\beta/3=x_N$, consistent with the result obtained previously. As $k$ is reduced $\varphi$ increases, becoming very small as $k$ approaches 1. (At $k=1$, however, [51] is no longer applicable since it predicts $\varphi(=\alpha)=0$, indicating that the condition [45], on which it is based, is no longer satisfied.) The corresponding value of $X$ is found by substitution of [51] in [21], making use of [45]:

$$\sin\varphi=\frac{2\beta R}{3X}, \qquad [52]$$

$$\frac{X}{R}=\frac{2\beta}{3}\sqrt{\left(\frac{k^2}{k^2-1}\right)}=\frac{2}{3}\frac{R^2}{a^2}\sqrt{\left(\frac{k^2}{k^2-1}\right)}. \qquad [53]$$

Note that with the help of [52] requirement [45] may be written

$$\frac{2\beta k}{3x}\gg 2x, \qquad \text{i.e.} \quad x<\sqrt{(2\beta k/3)}. \qquad [54]$$

Since [53] indicates that the largest $x$ values are obtained for values of $k$ close to unity, [54] requires that the largest $x$ values satisfy

$$x<\sqrt{(\beta/3)}, \qquad [55]$$

thus justifying the initial assumption that the plane of attachment lies in the neck region of the profile.

The bubble volume is obtained from [53]:

$$\frac{V_{max}}{a^3}\simeq\frac{4}{3}\pi\frac{R^3}{a^3}=2\pi\sqrt{\left(\frac{k^2-1}{k^2}\right)}\frac{X}{a}. \qquad [56]$$

Making use of [42], [56] may be written

$$\frac{V_{max}}{a^3}=\frac{2\pi r_0}{a}f \qquad [57]$$

where

$$f=\sqrt{\left(\frac{k^2-1}{k^2}\right)}[\tan(\varphi/2)]^{-1/k}. \qquad [58]$$

$f$ represents the factor by which the bubble volume is greater than that of a bubble formed on a sharp-edged orifice of radius $r_0$. Indeed with regard to bubble volume, the rounded orifice may

be seen as equivalent to a sharp-edged one of radius

$$r_{equ} = f r_0. \qquad [59]$$

Since $\varphi$ is determined by $k$ ([51]) so is $f$. As $k$ decreases from $\infty$ towards 1, $f$ increases from 1 towards 2. The effect of $k$ on the bubble volume, though quite noticeable, is thus not astronomical. If $k \leq 1$, $f$ could conceivably become much larger than 2 but since $\varphi$ is then very small the value of $f$ attained would depend critically on the exact shape of the orifice as it joins the adjacent plane surface. This is not pursued here.

## 4. INFLUENCE OF THE GROWTH RATE ON THE BUBBLE SIZE

*General force balance*

Considering mode A growth initially and defining "the bubble" as the gas lying within the control surface $S$ (figure 6), the following equation applies at all stages of growth, whether the bubble is formed rapidly or not†:

$$\mathbf{F} = \frac{d(\rho_G V \mathbf{u})}{dt} = \rho_G \frac{d(V\mathbf{u})}{dt} \qquad [60]$$

where $V$ is the bubble volume, $\mathbf{u}$ the velocity of its centre of gravity and $t$ denotes time. $F$ is the total force acting on the bubble and consists in general of:

$F_1$, the weight of the bubble $\rho_G V g$;
$F_2$, the surface tension force $2\pi r\sigma \sin\varphi$;
$F_3$, the force due to viscous stresses (normal and tangential) on $S$;
$F_4$, the force due to pressure variation over $S$ associated with any liquid flow;
$F_5$, the force due to the hydrostatic component of the pressure variation over $S$.

*The slow-formation case*

$F_5$ is equal to the Archimedes buoyancy force $\rho_L V g$, corrected for the fact that the hydrostatic pressure in that part of $S$ lying in the gas is in general different from the pressure in the liquid:

$$\begin{aligned} F_5 &= \rho_L V g + \pi r^2 (p_G - p_L)_{\text{orifice}} \\ &= \rho_L V g + \pi r^2 (2\sigma/R - \rho g h) \end{aligned} \qquad [61]$$

where $h$ is the height of the bubble (figure 6). For a bubble detaching under slow-formation conditions the relative magnitude of this correction term is

$$\begin{aligned} \frac{\pi r^2 (2\sigma/R - \rho g h)}{\rho_L V_{max} g} &= \frac{\rho V_{max} g (r/R)[1 - \beta(h/2R)]}{\rho_L V_{max} g} \\ &= \frac{2\rho}{3\rho_L} \beta[1 - \beta(h/2R)] = 0(\beta), \end{aligned} \qquad [62]$$

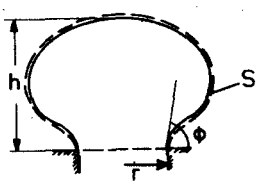


Figure 6. The control surface $S$.

†The momentum of the flow of liquid through $S$ required to satisfy vaporisation in the case of vapour bubbles is assumed negligible.

making use of [17], [15] and the fact that $h/2R = 0(1)$. The correction is thus small and, to the first approximation, may be neglected:

$$F_5 \simeq \rho_L V g. \qquad [63]$$

In addition $F_3$, $F_4$ and the R.H.S. of [60] are negligible and making use of [63] and the fact that $\varphi = 90°$ very nearly at detachment, [60] yields

$$\rho_G g V + 2\pi r\sigma = \rho_L V g,$$

leading to [17] and indicating that the buoyancy force $F_5$ and the surface-tension force $F_2$ are almost equal.

*The rapid-formation case*

When a bubble is formed rapidly the rise of the bubble leading to its detachment is impeded by the inertia of the surrounding liquid (i.e. $F_4$ becomes appreciable). The bubble therefore grows to a greater size before detaching and the buoyancy force becomes still larger while the correction term becomes smaller (since $R$ is larger: [61]). Approximation [63] thus becomes even better, while the surface tension term $F_2$ becomes small in comparison with the buoyancy term:

$$F_2 \ll F_5. \qquad [64]$$

Further, since $\rho_L \gg \rho_G$,

$$F_1 \ll F_5 \qquad [65]$$

and

$$\rho_G \frac{d(Vu)}{dt} \ll F_4, \qquad [66]$$

since, as will be seen,

$$F_4 \sim \rho_L \frac{d(Vu)}{dt}. \qquad [67]$$

Making use of [64], [65] and [66], [60] simplifies to

$$\mathbf{F}_3 + \mathbf{F}_4 + \mathbf{F}_5 = 0. \qquad [68]$$

For the present, the viscous force $F_3$ will also be assumed small in comparison with the other forces, yielding

$$\mathbf{F}_4 + \mathbf{F}_5 = 0. \qquad [69]$$

The resistive inertial force $F_4$ acting on a sphere accelerating in an unbounded inviscid liquid can be shown to be

$$\mathbf{F}_4 = -\frac{d(m_{virt}\mathbf{u})}{dt}, \qquad [70]$$

where the "virtual mass" $m_{virt}$ is given by (Milne-Thomson 1968)

$$m_{virt} = \frac{1}{2}\rho_L V. \qquad [71]$$

Although the actual bubble will not be completely spherical and grows in liquid bounded on the underside, the general trends and orders of magnitude predicted by [70] and [71] (which lead to [67]) may be expected to be correct.

Davidson & Harrison (1963) have shown that for the case of a constant growth rate,

$$\frac{dV}{dt} = G = \text{constant}, \qquad [72]$$

substitution of [63], [70] and [71] in [69] leads to

$$u = gt$$

and

$$V_{max} = \left(\frac{6}{\pi}\right)^{1/5} \frac{G^{6/5}}{g^{3/5}}, \qquad [73]$$

the criterion of detachment being that the height of the bubble centre above the orifice becomes equal to $R$.

Since [73] no longer includes surface-tension effects it may also be expected to apply to mode B growth at sufficiently high growth rates.

For bubbles formed at high, constant gas flow rates on vertical tubes [73] provides a surprisingly good prediction of the observations (Davidson & Harrison 1963). Since $V_{max}$ increases almost linearly with $G$ the bubble frequency remains approximately constant.

*Transition from slow to rapid formation*

An indication of the value of $G$ at which $V_{max}$ begins to increase significantly should be provided by the point $P$ (figure 7) at which the bubble size predicted by [73] equals that predicted by the slow-formation theory:

$$\left(\frac{6}{\pi}\right)^{1/5} \frac{G_{crit}^{6/5}}{g^{3/5}} = \frac{2\pi r\sigma}{\rho g} \quad \text{(mode A†)} \qquad [74]$$

or

$$= (0.0172\, a\varphi_0)^3 \quad \text{(mode B)}. \qquad [75]$$

In the case of vapour bubbles formed during nucleate pool boiling the growth rate is governed by thermal conduction, except initially or at sub-atmospheric pressures, and the order of magnitude of $G$ may be obtained from the simple expression for the conduction-governed growth of a bubble in an initially uniformly superheated region (Plesset & Zwick 1954):

$$R = \mathrm{B}\sqrt{t} \qquad [76]$$

giving

$$G = 4\pi R^2 \frac{dR}{dt} = 2\pi \mathrm{B}^2 R \qquad [77]$$

where

$$2\pi \mathrm{B}^2 = 24 k_L \rho_L c_L (\Delta T / i\rho_G)^2 \qquad [78]$$

†For a round-edged orifice, $r$ must be replaced by $r_{equ}$: [59].

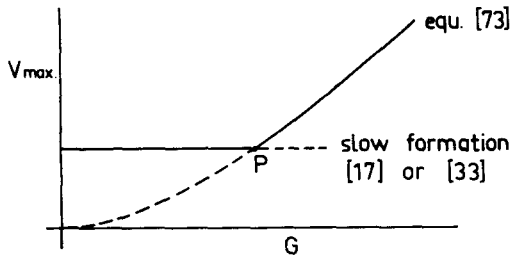


Figure 7. Onset of inertial effects in bubble growth.

($k_L$, $c_L$, $i$ and $\Delta T$ respectively liquid thermal conductivity and specific heat, latent heat of vaporisation and liquid superheat).

Consistent with the approximation of uniform superheat $\Delta T$, the value of $\Delta T$ is related to the cavity radius $r$ ($r_0$ for the case of a well-wetted, round-edged cavity) by the well-known relation

$$\Delta T = \frac{T}{i\rho_G}\frac{2\sigma}{r}, \qquad [79]$$

where $T$ denotes the absolute temperature, and the specific volume of the liquid $1/\rho_L$ has been neglected in comparison with that of the vapour, $1/\rho_G$.

In defence of the uniform-superheat approximation it should be remarked that while a steep variation of temperature with distance from the wall in general exists in the undisturbed liquid, in the immediate vicinity of a vapour bubble this variation is far less pronounced (Beer 1971) since the vapour bubble acts as a heat pipe, with a strong tendency to eliminate temperature variations over its surface. The fairly uniform surface temperature thus obtained is of course considerably lower than the wall temperature.

Combining [77]–[79],

$$G = \frac{K_1 R}{\rho_G^4 r^2} \qquad [80]$$

where

$$K_1 = 96 k_L \rho_L c_L (T\sigma/i^2)^2. \qquad [81]$$

Substitution of [80] in [74] making use of [16] for $R$, or in [75] making use of [32] for $R$, gives

$$r_{crit}^{5/2}\rho_G^4 = K_2 \quad \text{(mode A)}, \qquad [82]$$

where:

$$K_2 = K_1/[\pi(8/3)^{1/3} a g^{1/2}] \qquad [83]$$

and

$$r_{crit}^2\rho_G^4 = K_3 \quad \text{(mode B)}, \qquad [84]$$

where

$$K_3 = 0.0107(6/\pi)^{1/6} K_1/[(0.0172)^{5/2} g^{1/2}(a\varphi_0)^{3/2}]. \qquad [85]$$

The implications of the above equations are most easily illustrated by an example. For a given liquid $K_1$, $K_2$ and $K_3$ are approximately constant. For water $K_2 = 1.3 \times 10^{-13}$ kg$^4$ m$^{-19/2}$ based on its physical properties at 100°C, and for mode A growth at atmospheric pressure [82] yields $r_{crit} = 16\,\mu$. For cavities of this order or larger therefore, growth will be approximated by the slow-formation theory, the bubble volume increasing linearly with the cavity dimension [17]. Cavities appreciably smaller than 16 $\mu$ in radius will grow bubbles according to the rapid

growth theory:

$$R^3 \propto V_{max} \propto G^{6/5} \propto \left(\frac{R}{r^2}\right)^{6/5}, \quad \text{from [73] and [80]}$$

$$R \propto r^{-4/3} \qquad [86]$$

$$V_{max} \propto r^{-4}. \qquad [87]$$

The bubble volume thus increases (rapidly) as $r$ decreases. The bubbles of minimum volume will evidently be formed on cavities of radius $\sim 16\,\mu m$.

The influence of increased pressure is to raise $\rho_G$ and hence to lower the value of $r_{crit}$:

$$r_{crit} \propto \rho_G^{-8/5} \propto p_{abs}^{-8/5}. \qquad [88]$$

At high pressures the value of $r_{crit}$ is thus likely to be so low that growth on all active cavities is governed by the slow-formation theory.

Essentially the same results are obtained for mode B growth, the value of $r_{crit}$ being different, but of the same order.

Before passing on to viscous and thermal effects a possible flaw in the foregoing reasoning should be checked out. It is known that the initial, dynamically-controlled growth of bubbles often produces a flattening of the bubble into a hemispherical form (figure 8). The "microlayer" of liquid between bubble and wall then partially evaporates, leaving the three-phase contact line outside the cavity during further growth. In appendix 1, however, it is demonstrated that the condition that final growth should be "slow" is also a sufficient condition that microlayer formation should not take place. This conclusion is confirmed experimentally.

## 5. THE INFLUENCE OF VISCOSITY ON BUBBLE GROWTH

In the absence of externally imposed liquid flow (forced convection) the influences of viscosity on vapour bubble growth are of three types: (1) normal viscous stresses associated with the expansion of the bubble; (2) tangential viscous stresses associated with surface-tension gradients; (3) viscous effects associated with the rise of the bubble ("drag").

Since, as already noted, expansion is in general controlled by thermal conduction rather than dynamic effects, influence 1 is not likely to be of interest here. Influence 2 is considered in the next section.

Influence 3, the drag force, is of possible importance at high growth rates. In the first place it is worth noting that this force probably changes sign during the course of bubble growth since initially the wake of the previous, departing bubble causes an updraft of liquid. This in itself reduces the net effect.

The drag force on an approximately spherical bubble at Reynolds numbers considerably greater than unity is smaller than that on a solid sphere since the flow does not separate (Moore 1963):

$$\mathbf{F}_{drag} = -12\pi\mu_L R\mathbf{u} \qquad [89]$$


Figure 8. Early stages of bubble growth (a) surface tension dominant (b) liquid pressure dominant.

where $\mu_L$ is the dynamic viscosity. Equation [89] neglects the possible influence of expansion on the drag, as indeed is done in the case of a rising bubble. This may be expected to be reasonable provided the radial velocity, $u_r$, is small in comparison with the rise velocity, $u$. Assuming the correct order of magnitude of these velocities to be given by the theory of the preceding section.

$$u_r = \frac{dR}{dt} = \frac{G}{4\pi R^2}$$

and

$$u = \sqrt{(2gR)}, \qquad [90]$$

since the bubble centre accelerates at $g$, so that

$$\frac{u_r}{u} = \frac{1}{4\pi\sqrt{2}} \cdot \frac{G}{R^2\sqrt{(gR)}}. \qquad [91]$$

However, substitution of $V_{max} = \frac{4}{3}\pi R^3$ in [73] indicates that at detachment,

$$\frac{G}{R^2\sqrt{(gR)}} = \frac{4\pi\sqrt{2}}{6} \qquad [92]$$

so that [91] gives

$$\frac{u_r}{u} = \frac{1}{6} \qquad [93]$$

and [89] should be a good approximation. Comparing $F_{drag}$ with the buoyancy force $F_5$,

$$\frac{F_{drag}}{F_5} = \frac{12\pi\mu_L R u}{4/3\pi R^3 \rho_L g}.$$

making use of [90] the value of this ratio at departure of the bubble is found to be

$$\frac{F_{drag}}{F_5} = \frac{18\mu_L}{\rho_L R\sqrt{(2gR)}} = \frac{18}{Re}. \qquad [94]$$

where $Re$ is the Reynolds number at detachment, based on the bubble radius. In general $R \geq 0.5$ mm. Taking the example of water at 100°C, [94] thus yields $F_{drag}/F_5 \leq 0.1$ (and $Re \geq 180$, validating the use of [89]). The influence of $F_{drag}$ is thus likely to be minor in the case of water and other low-viscosity liquids.

## 6. THE INFLUENCE OF SURFACE-TENSION GRADIENTS

A vapour bubble acts as a heat pipe, tending to equalize the temperature over its surface. Some variation however, of the order of 1°C, remains (Beer 1971). The resulting surface-tension gradients produce a net force on an element of surface which has to be balanced by a shear stress, $\tau$, exerted by the adjacent liquid since the mass of "the surface" is negligible. The surface moves in such a way as to produce this shear stress and in fact jets the adjacent layer of liquid away from the wall (figure 9). The resultant viscous force on the bubble (directed

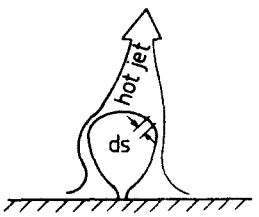


Figure 9. Production of hot jets by surface-tension gradients.

towards the wall) is:

$$F_{ST} = \int \tau \sin\theta \, 2\pi X \, ds$$

$$= \int \frac{d\sigma}{ds} \sin\theta \, 2\pi X \, ds$$

$$= \int 2\pi X \sin\theta \, d\sigma \sim R\Delta\sigma \qquad [95]$$

where $ds$ is the width of an annular strip of the surface (figure 9), and $\Delta\sigma$ is the surface-tension difference between top and bottom of the bubble.

Comparing $F_{ST}$ with the buoyancy force $F_S$,

$$\frac{F_{ST}}{F_S} \sim \frac{R\Delta\sigma}{\frac{4}{3}\pi R^3 \rho_L g} \sim \frac{\Delta\sigma}{4R^2\rho_L g}. \qquad [96]$$

For water at 100°C, with $R \geq 0.5$ mm and $\Delta\sigma$ corresponding to 1°C, [96] gives $F_{ST}/F_S \leq 0.02$, indicating that $F_{ST}$ may safely be neglected in the first approximation.

## 7. COMPARISON WITH POOL BOILING RESULTS

*Boiling on large, sharp-edged cavities at atmospheric pressure*

Howell & Siegel (1966) produced bubbles in water at atmospheric pressure on artificial, circular, sharp-edged cavities in heated steel strips. The cavity radii ranged from 50 to 500 $\mu$m and in all cases growth was according to mode A. In accordance with the preceding theory, both the profiles and departure volumes of the bubbles agreed well with the slow-formation theory.†

The fact that mode A occurred, however is anomolous: according to [36] mode A growth requires that $\varphi_0 < 15°$, whereas Ponter *et al.* (1967*a*, 1967*b*) found $\varphi_0 = 65°$ at 20°C and affirmed that $\varphi_0$ varies but slowly with temperature. The explanation probably lies in the well-known slowness of a contact angle to adjust itself to its equilibrium value when this involves the macroscopic motion of the three-phase boundary over a solid surface. The time available for this motion may be obtained as follows.

From [76], making use of [77], [80], [82] and [83], the total growth time of the bubble, $t_{gr}$, is given by

$$t_{gr} = R^2/B^2$$

$$= 2\pi R^3/G$$

$$= 2\pi R^2 \rho_G{}^4 r^2 / K_1$$

$$= \frac{3^{1/3} R^2 r^2}{a g^{1/2} r_{crit}^{5/2}}. \qquad [97]$$

†Since, however, the population of artificial sites was very sparse, the effective value of $\Delta T$ would be expected to be higher than that given by [79], though still smaller than $T_{wall} - T_{sat.}$. This is borne out by the measured growth rates. The corresponding value of $r_{crit}$ is thereby somewhat increased.

From [16] and [19],

$$R = (3ra^2/2)^{1/3} \qquad [98]$$

and [97] may be re-written

$$t_{gr} = \frac{3(a/4)^{1/3} r_{crit}^{1/6}}{g^{1/2}} \left(\frac{r}{r_{crit}}\right)^{8/3}$$

$$= K_4 (r/r_{crit})^{8/3} \qquad [99]$$

where

$$K_4 = 3(a/4)^{1/3} r_{crit}^{1/6}/g^{1/2}. \qquad [100]$$

For slow growth $r$ must be greater than $r_{crit}$ and for a given liquid and a given $r/r_{crit}$ value, $t_{gr}$ is seen to be approximately independent of the condition of boiling (i.e. of the pressure), since $K_4$ is insensitive to the values of $a$ and $r_{crit}$. For water, $K_4 \sim 10^{-2}$ s, based on the value of $r_{crit}$ (16 $\mu$) found previously for atmospheric pressure. Only a fraction of $t_{gr}$ is available for expansion of the three-phase boundary (i.e. during only a fraction of $t_{gr}$ is $\varphi$ less than $\varphi_0$).

In the appendix 2 it is shown that except for very small values of $\varphi_0 (\lesssim 10°)$

$$\frac{\Delta V}{V_{max}} = \sin \varphi_0, \qquad [101]$$

where $\Delta V$ is the increase in bubble volume during the phase of growth in which $\varphi < \varphi_0$. For $\varphi_0 \geq 90°$, all of $t_{gr}$ is therefore available for expansion of the three-phase boundary; for smaller $\varphi_0$ the time available, $t_{exp}$, is smaller, but of the same order:

$$t_{exp} \simeq \sin \varphi_0 K_4 (r/r_{crit})^{8/3}$$

$$\simeq K_5 (r/r_{crit})^{8/3}, \qquad [102]$$

where

$$K_5 = \sin \varphi_0 K_4. \qquad [103]$$

The experiments of Howell & Siegel suggest that $t_{exp}$ is insufficient for mode B growth to occur up to $r/r_{crit} \sim 30 (= 500\ \mu/16\ \mu)$ for $\varphi_0 \simeq 65°$.

*Boiling on large natural cavities at atmospheric pressure under normal and reduced gravity*

The size and shape of bubbles formed in water at atmospheric pressure on natural nucleation sites in a nickel surface was studied by Siegel & Keshock (1964) under normal and reduced gravity. Although attempt was made to correlate the results with the mode B formula [32], it is evident from the photographs that the bubbles did not spread beyond the cavities. This is illustrated in figure 10 by the tracings of a bubble growing in 6.1% of normal gravity. The final bubble size leads to $\beta = 0.134$ and according to mode B theory the contact diameter with the heating surface should then be 0.3 times the bubble diameter. In reality the contact diameter is virtually constant during growth and accords much better with the value of 0.09 times the final

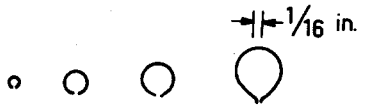


Figure 10. Bubble growth in reduced gravity (Siegel & Keshock 1964).

diameter predicted by mode A theory. The corresponding cavity radius proves to be 340 $\mu$m, confirming that the slow-formation theory should apply. In the absence of contact-angle data on nickel surfaces no statement can be made about which mode should have occurred according to the criterion [36].

A further, indirect confirmation of the mode A growth is the $g$ dependence of $R_{\text{final}}$. For mode A this should be

$$R_{\text{final}} \propto g^{-1/3} \qquad [104]$$

and for mode B

$$R_{\text{final}} \propto g^{-1/2}. \qquad [105]$$

The observations are best approximated by [104] down to $g \sim 10\%$ normal, after which successive bubbles tend to merge.

The fact that the authors nevertheless successfully correlated the bubble departure diameters with the mode B, equation [32] demands an explanation. In this and many other experiments, the angle $\varphi$ (figure 3b) was interpreted by the experimenters as the natural contact angle $\varphi_0$, despite its variation during growth and from site to site. The value assigned to $\varphi_0$ in [32] was that observed just prior to departure. Since the dimensions of the neck region are so small ($\sim \beta R$) that it is barely visible this value of $\varphi_0$ was probably close to that in the last, fairly straight portion of the profile, namely $\varphi_I$.† This, coincidentally, is exactly the contact angle required to obtain agreement with the mode B theory since the final plane of attachment in mode B growth is the plane of the point $I$ ([29]).

*Boiling at low pressures*

Experiments at pressures well below atmospheric indicate that bubbles formed on all cavities are very large (e.g. Cole & Shulman 1966), confirming the implications of [82] and [84] that $r_{\text{crit}}$ becomes very large. Since growth is not "slow" these results are not discussed further here.

*Boiling on natural cavities at high pressures*

The average size of the bubbles formed on various metal surfaces at atmospheric and higher pressures was measured by Tolubinsky & Ostrovsky (1966). The heat fluxes used were low in order to produce few active cavities. The results for water are reproduced in figure 11 and agree, globally, with the expectations. Thus, the bubble size falls off sharply at first and then

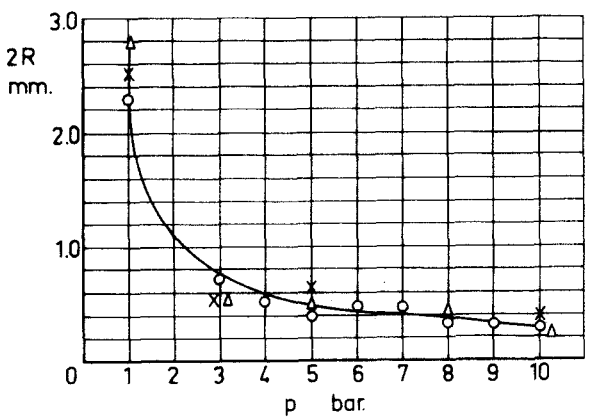


Figure 11. Bubble departure sizes at high pressures (Tolubinsky & Ostrovsky 1966).

†The authors themselves say that "it was very difficult to make accurate contact angle measurements because extreme clarity and high magnification are required before one can tell whether the actual contact angle at the root of the bubble is being measured rather than the slope of the bubble close to the root".

levels off, as would be expected if growth becomes governed by the slow-formation theory. A certain residual slope is to be expected due to the decrease of surface tension with temperature but the actual slope is too great to be explained solely by this effect. The possibility suggests itself that the larger cavities fill up under the influence of the pressure and that, to maintain the heat flux, the superheat increases and smaller cavities become active. Certainly the authors state that more cavities are active at the higher pressures, and the assumption of mode A growth leads to cavity sizes of less than 1 $\mu$m at the highest pressures. In view of such possible complications no further conclusions can be drawn.

## 8. CONCLUSIONS

(1) The size of a gas bubble formed slowly on a round, sharp-edged horizontal orifice under isothermal conditions depends on whether the bubble remains confined to the orifice ("mode A") or spreads beyond it ("mode B"). This in turn is decided by the magnitude of the natural contact angle $\varphi_0$ ([36]). For small orifices simple analytic expressions for the bubble volumes may be obtained ([17] and [33]), that for mode B agreeing with the well known numerical result of Fritz (1935).

(2) The situation for round-edged orifices is similar, the size of the bubble formed in mode A growth (in which the contact radius of the bubble changes during growth but remains within the orifice) being the same as that formed on a sharp-edged orifice of somewhat larger radius, $r_{equ}$ ([59]).

(3) For sufficiently high growth rates the inertial forces associated with acceleration of the surrounding liquid become of influence and the bubble volume begins to increase with increasing growth rate. For vapour bubbles formed in nucleate pool boiling inertial forces are important if the cavity radius is less than, or of the order of, that given by [82] (mode A) or [84] (mode B). Growth may be expected to be "slow" on most cavities at high pressures and "rapid" on most at low pressures.

(4) The criterion for growth to be "slow" is also a sufficient condition for microlayer formation not to occur.

(5) The influences of viscous forces and surface-tension gradients on bubble growth may in general be expected to be slight for low-viscosity liquids such as water.

(6) Data on nucleate pool boiling of water confirm the above expectations with the exception that mode B is not obtained under conditions when it would be expected (i.e. "slow" growth, with $\varphi_0$ considerably greater than the minimum contact angle attained). This is attributed to the well known slowness of spreading of a three-phase boundary. An analysis of the time available for spreading indicates that this is of the same order at all pressures for a given value of $r/r_{crit}$ (the ratio which determines whether growth is "slow" or not) and it thus appears likely that the Fritz mode of growth (mode B), on which so many heat transfer correlations are based, never in fact occurs in the case of water. If so, the same conclusion would be expected to apply to low-viscosity organic liquids.

## REFERENCES

BASHFORTH, F. & ADAMS, H. 1883 *The Theories of Capillary Action.* Cambridge Univ. Press, Cambridge.

BEER, H. 1971 Das dynamische Blasenwachstum beim Siedem von Flüssigkeiten an Heizflächen. *Forsch. Geb. Ing Wes.* **37**, 85–90.

CHESTERS, A. K. 1977 An analytical solution for the profile and volume of a small drop or bubble symmetrical about a vertical axis. *J. Fluid Mech.* **81**, 609–624.

COLE, R. & SHULMAN, H. L. 1966 Bubble growth rates at high Jakob numbers. *Int. J. Heat Mass Transfer* **9**, 1377–1390.

DAVIDSON, J. & HARRISON, D. 1963 *Fluidized Particles*, Chap. 3. Cambridge Univ. Press, Cambridge.

DAVIES, J. T. & RIDEAL, E. K. 1963 *Interfacial Phenomena*, 2nd Edn, p. 35. Academic Press, New York.

FRITZ, W. 1935 Berechnung des maximale Volume von Dampfblasen. *Phys. Z.* **36**, 379–384.

HARTLAND, S. & HARTLEY, R. W. 1976 *Axisymmetric Fluid–Fluid Interfaces*. Elsevier, Amsterdam.

HOWELL, J. R. & SIEGEL, R. 1966 Incipience, growth and detachment of boiling bubbles in saturated water from artificial nucleation sites of known geometry and size, Proc. 3rd Int. Heat Transf. Conf., Chicago, Vol. IV, 12–33.

JOHNSON, M. A., DE LA PENA, J. & MESLER, R. B. 1966 Bubble shapes in nucleate pool boiling, *A.I.Ch.E.Jl* **12**, 344–348.

MICHAEL, D. H. & WILLIAMS, P. G. 1976 The equilibrium and stability of axisymmetric pendent drops. *Proc. R. Soc. Lond.* A **351**, 117–127.

MILNE-THOMSON, L. M. 1968 *Theoretical Hydrodynamics*, 5th Edn, Section 16.32. Macmillan, London.

MOORE, D. W. 1963 The boundary layer on a spherical gas bubble. *J. Fluid Mech.* **16**, 161–176.

PITTS, E. 1976 The stability of a drop hanging from a tube. *J. Inst. Math. Appl.* **17**, 387–397.

PLESSET, M. S. & PROSPERETTI, A. 1977 Bubble dynamics and cavitation. *A. Rev. Fluid Mech.* **9**, 145–185.

PLESSET, M. & ZWICK, S. A. 1954 The growth of vapour bubbles in super heated liquids. *J. Appl. Phys.* **25**, 493–500.

PONTER, A. B. & DAVIES, G. A., ROSS, T. K. & THORNLEY, P. G. 1967*a* The influence of mass transfer on liquid film breakdown. *Int. J. Heat Mass Transfer* **10**, 349–359.

PONTER, A. B., DAVIES, G. A., ROSS, T. K. & THORNLY, P. G. 1967*b* The measurement of contact angles under conditions of heat transfer when a liquid film breaks on a vertical surface. *Int. J. Heat Mass Transfer* **10**, 1633–1636.

SIEGEL, R. & KESHOCK, E. G. 1964 Effects of reduced gravity on nucleate boiling bubble dynamics in saturated water. *A.I.Ch.E.Jl* **10**, 509–517.

TOLUBINSKY, V. I. & OSTROVSKY, J. N. 1966 On the mechanism of boiling heat transfer (vapour bubbles growth rate in the process of boiling of liquids, solutions and binary mixture). *Int. J. Heat Mass Transfer* **9**, 1463–1470.

VACEK, V. & NEKOVAR, P. 1973 A note on residual drop and single drop formation. *Appl. Sci. Res.* **28**, 134–144.

# APPENDIX 1

## MIROLAYER FORMATION IN EARLY STAGES OF GROWTH

*Criterion for microlayer formation*

Microlayer formation is a result of deformation of the bubble from the spherical by the liquid-pressure distribution over its surface associated with its growth† (figure 8).

An appropriate criterion for the formation of a microlayer should therefore be

$$\Delta p \gg 2\sigma/R, \qquad [A1.1]$$

where $\Delta p$ is the order of the liquid-pressure variation over the bubble surface. $\Delta p$ may also be expressed as

$$\Delta p = (p_A - p_\infty) - (p_B - p_\infty)$$

where $A$ and $B$ are two widely separated points on the bubble surface and $p_\infty$ is the pressure in the undisturbed liquid far away.

†For simplicity the additional pressure variation due to gravity is ignored.

Since $p_A - p_\infty$ and $p_B - p_\infty$ are of the order of $\rho_L \dot{R}^2$ where $\dot{R}$ is the order of the radial expansion velocity,

$$\Delta p \leq \rho_L \dot{R}^2 \qquad [A1.2]$$

and [A1.1] becomes

$$\rho_L \dot{R}^2 \gg 2\sigma/R. \qquad [A1.3]$$

*Magnitude of* $\dot{R}$

The order of magnitude of the terms in [A1.3] may be obtained from their values for a spherically symmetrical expansion. Three regimes will be considered.

(1) $R \gg R_0$, but expansion still dynamically controlled.

Then (Plesset & Prosperetti 1977),

$$\Delta p \simeq \frac{2\sigma}{R_0} = \frac{3}{2}\rho_L \dot{R}^2. \qquad [A1.4]$$

$\dot{R}$ is thus constant. [A1.1] and [A1.4] yield

$$2\sigma/R_0 \gg 2\sigma/R,$$

i.e.

$$R/R_0 \gg 1$$

or

$$R/r \gg 1 \qquad [A1.5]$$

since in the context of wall growth $R_0 = r$ (the cavity radius). This criterion for microlayer formation is thus satisfied if the dynamically-controlled regime persists to $r$ values much greater than the cavity radius.

(2) $R \gg R_0$, and expansion thermally controlled.

Then (Plesset & Prosperetti 1977),

$$R = K\sqrt{t}$$

and

$$\dot{R} = K/2\sqrt{t} = K^2/2R, \qquad [A1.6]$$

where $K$ is a constant depending on the cavity radius and the liquid and vapour properties.

Substitution of [A1.6] in [A1.3] yields

$$\frac{\rho_L K^2}{2R^2} \gg \frac{2\sigma}{R}. \qquad [A1.7]$$

The L.H.S. diminishes more rapidly with increasing $R$ than the R.H.S. so if microlayer formation has not yet occurred on entering the thermally-controlled regime, it never will.

(3) $R \gg R_0$, transition from dynamic to thermal control.

At transition,

$$\dot{R}_{\text{dynamic}} \sim \dot{R}_{\text{thermal}}.$$

Hence, from [A1.4] and [A1.6]

$$\sqrt{\left(\frac{4\sigma}{3\rho_L R_0}\right)} \sim \frac{K^2}{2R},$$

i.e.

$$R/r \sim \frac{K^2}{4}\sqrt{\left(\frac{3\rho_L}{\sigma r}\right)} \quad \text{or} \quad R/r \sim \frac{K^2}{4}\sqrt{\left(\frac{3\rho_L}{\sigma r}\right)}. \qquad [A1.8]$$

The transition point provides the largest $R$ value in the dynamic regime and so the greatest chance of microlayer formation.

Substitution of [A1.8] in [A1.5] results in

$$K^2 \gg 4\sqrt{(\sigma r/3\rho_L)}. \qquad [A1.9]$$

*Magnitude of* K *in the slow-formation regime*

The volume growth rate, $G_{crit}$, at which the slow-formation model breaks down is given by [74] or [75]:

$$\left(\frac{6}{\pi}\right)^{1/5} \frac{G_{crit}^{6/5}}{g^{3/5}} = V_{max} = \frac{4}{3}\pi R_{max}^3. \qquad [A1.10]$$

From [A1.6],

$$G = 4\pi R^2 \dot{R} = 2\pi K^2 R. \qquad [A1.11]$$

Substitution of [A1.11] in [A1.10] yields

$$K^2 = \frac{\sqrt{(2g)}}{3} \cdot R_{max}^{3/2} = \sqrt{\left(\frac{g}{6\pi}\right)} \cdot V_{max}^{1/2}. \qquad [A1.12]$$

For mode A growth ([17]),

$$V_{max} = 2\pi r\sigma/\rho g \simeq 2\pi r\sigma/\rho_L g \qquad [A1.13]$$

and [A1.12] becomes

$$K^2 = \sqrt{(r\sigma/3\rho_L)}. \qquad [A1.14]$$

The condition that the slow-formation theory be valid is thus

$$K^2 \ll \sqrt{(r\sigma/3\rho_L)}. \qquad [A1.15]$$

## CONCLUSION

From [A1.9] it is seen that [A1.15] is a sufficient criterion for microlayer formation not to occur. Evidently under the conditions concerned in the slow-formation regime, growth is thermally controlled from the beginning. This is not surprising since for typical cavity sizes the pressures involved are atmospheric and upwards.

In the case of mode B growth [A1.13] can be replaced by

$$V_{max} = (0.0172\, a\varphi_0)^3 = n(2\pi r\sigma/\rho_L g) \qquad [A1.13']$$

yielding

$$K^2 \ll \sqrt{(nr\sigma/3\rho_L)}. \qquad [A1.15']$$

For $\varphi_0 \lesssim 30°$, as assumed in the various expressions in the main body of the paper, and typical cavity sizes, $\sqrt{n}$ is found to be of the order of unity and the same conclusion therefore applies.

These conclusions are confirmed by the observations of Johnson *et al.* (1966) that bubbles formed in water are round or only slightly distorted at atmospheric pressure and only become hemsipherical at low pressures.

# APPENDIX 2

## FRACTIONAL GROWTH WHILE $\varphi < \varphi_0$

For mode A growth and values of $\varphi_0$ greater than 90°, $\varphi$ becomes smaller than $\varphi_0$ in the early stages of growth and remains so (figure 4a). For $\varphi_0 < 90°$, $\varphi$ again falls below $\varphi_0$ in the early stages of growth, reaches a minimum and then rises above $\varphi_0$ before detachment occurs (at which point $\varphi = 90°$). The second point at which $\varphi$ becomes equal to $\varphi_0$ occurs after $\varphi_{min}$ has been reached and the plane of attachment therefore lies in the neck region. From [21], therefore,

$$\sin \varphi_0 = \frac{r}{R_2} + \frac{2\beta_2 R_2}{3r}$$

yielding

$$\frac{r}{R_2} = \frac{\sin \phi_0 \pm \sqrt{(\sin^2 \varphi_0 - 8\beta_2/3)}}{2}. \qquad [A2.1]$$

Except for very small $\varphi_0$ values ($\varphi_0 \sim \varphi_I \sim 10°$)

$$\sin^2 \varphi_0 \gg 8\beta_2/3 \qquad [A2.2]$$

and [A2.3] reduces to

$$\frac{r}{R_2} = \frac{\sin \varphi_0}{2}[1 \pm (1 - (4\beta_2/3)/\sin^2 \varphi_0)] \qquad [A2.3]$$

$$= \frac{2\beta_2}{3 \sin \varphi_0}, \qquad [A2.4]$$

the negative sign applying on the neck side of the inflexion point, $I$ (figure 1). Re-arranging [A2.4],

$$V_2 \simeq \frac{4}{3}\pi R^3 = 2\pi r a^2 \sin \varphi_0 \qquad [A2.5]$$

and from [18] (or from [A2.5] with $\varphi_0 = 90°$),

$$V_2 / V_{max} = \sin \varphi_0. \qquad [A2.6]$$

Choice of the positive sign in [A2.3] yields the point at which $\varphi$ first becomes equal to $\varphi_0$, when the plane of attachment lies on the apex side of the inflexion point $I$. For large values of $\varphi_0$ use of the neck solution in this case gives only an order of magnitude for the corresponding bubble volume $V_1$ but this is sufficient since $V_1$ will be seen to be negligible. Thus, from [A2.3],

$$\frac{r}{R_1} = \sin \varphi_0$$

yielding

$$V_1 \lesssim \frac{4}{3}\pi (r/\sin \varphi_0)^3$$

and

$$V_1/V_2 \lesssim \frac{3}{2}\frac{r^2}{a^2 \sin^2 \varphi_0}. \qquad \text{[A2.7]}$$

Since $r \ll a$ and $\sin \varphi_0 = 0(1)$

$$V_1/V_2 \ll 1$$

and

$$\frac{\Delta V}{V_{max}} = \frac{V_2 - V_1}{V_{max}} \simeq \frac{V_2}{V_{max}} = \sin \varphi_0. \qquad \text{[A2.8]}$$

For $\varphi_0 \geq 90°$, $V_2 = V_{max}$ and $\Delta V/V_{max} \simeq 1$.